Field line diffusion and loss in a tokamak with an ergodic magnetic limiter

Elton C. da Silva and Iberê L. Caldas
Instituto de Física, Universidade de São Paulo, C.P. 66318, 05315-970, São Paulo, São Paulo, Brazil

Ricardo L. Viana[a]
Departamento de Física, Universidade Federal do Paraná, C.P. 19081, 81531-990,
Curitiba, Paraná, Brazil

A numerical study of chaotic field line diffusion in a tokamak with an ergodic magnetic limiter is described. The equilibrium model field is analytically obtained by solving a Grad–Schlüter–Shafranov equation in toroidal polar coordinates, and the limiter field is determined by supposing its action as a sequence of delta-function pulses. A symplectic twist mapping is introduced to analyze the mean square radial deviation of a bunch of field lines in a predominantly chaotic region. The formation of a stochastic layer and field diffusivity at the plasma edge are investigated. Field line transport is initially subdiffusive and becomes superdiffusive after a few iterations. The field lines are lost when they collide with the tokamak inner wall; their decay rate is exponential with Poisson statistics. © *2001 American Institute of Physics.* [DOI: 10.1063/1.1371769]

I. INTRODUCTION

The existence of magnetic surfaces is a necessary requirement for plasma confinement in fusion schemes.[1,2] These surfaces, with the topology of nested tori, exist whenever the system has some spatial symmetry and, accordingly, they may well be destroyed as this symmetry is broken by some means.[3] The problem of particle confinement in a plasma is related in a nonobvious way to the problem of determination of magnetic surfaces. Classical and neoclassical transport in a direction perpendicular to these surfaces, for example, is not sufficient to explain the experimental data.[4,5] This phenomenon of anomalous transport has been one of the most studied themes in fusion plasma theory since the 1960s.[6]

There are two general points of view on anomalous diffusion: (i) the existence of magnetic surfaces is assumed, but the transport properties are due to complex particle motions which are disregarded in traditional theories; (ii) the particle orbits are taken as essentially simple, but the magnetic surfaces themselves may not exist.[7] In the latter case, a layer of stochastic, or chaotic, magnetic field lines should be found. These chaotic field lines are volume filling in an essentially ergodic fashion, causing a uniform spread of particles and energy. Field lines in a magnetostatic configuration may be chaotic in a Lagrangian sense—nearby field lines diverge exponentially in their revolutions along the torus.

One of the first works to deal with this problem was the seminal paper of Rosenbluth *et al.*,[8] in which it was assumed that the destruction of magnetic surfaces is caused by a symmetry-breaking resonant perturbation. Since then, this problem has been extensively studied in fusion[9–11] and astrophysical applications.[12] Magnetic surface destruction is related to the overlapping of two or more chains of magnetic islands.[13,14] These islands may result from the interaction between two helical resonant magnetostatic perturbations, or from one helical perturbation with toroidal effects.[9] The destruction of magnetic surfaces is followed by the appearance of a thin layer of chaotic magnetic field lines in the neighborhood of the islands' separatrices. These layers may fuse and spread out throughout a larger region, if the perturbation is strong enough.

While field line chaos may sometimes be regarded as an undesirable feature—as it may trigger soft disruptive instabilities in tokamaks, e.g., Refs. 15 and 16—it can be of interest for the sake of controlling plasma–wall interactions in tokamaks. It has been proposed that a cold boundary layer of chaotic field lines may uniformize heat and particle loadings on the tokamak inner wall,[17] reducing the release of impurities due to sputtering processes. More specifically, it has been argued that the impurity concentration in the plasma core could be reduced by a factor that is inversely proportional to the electron diffusion coefficient in the plasma edge.[18]

This chaotic region in the plasma edge may be created using suitably designed resonant helical windings,[19] but they have to be mounted externally to the tokamak vessel wall, which is an intensively used interface with many diagnostic windows that complicate the task of setting up these windings. The ergodic magnetic limiter (EML), on the other hand, circumvents this problem by using only slices of helical windings in the form of current rings.[20] Some experiments with EMLs[21,22] have shown a decrease of the plasma temperature in the edge region, thus reducing plasma–wall interactions, as well as opening the possibility of controlling some magnetohydrodynamical (MHD) oscillation modes. However, the claim that the chaotic boundary layer could uniformize heat and particle loadings in the wall has been questioned by experiments in which a poloidal modulation of thermal fluxes has been observed.[23,24]

The design of an EML depends on a detailed knowledge

---

[a]Electronic mail: viana@fisica.ufpr.br

of the field line diffusion in the chaotic region it is supposed to generate. In this paper we aim to study field line diffusion in a tokamak with EML, in order to investigate the design parameters required to achieve efficient particle diffusion in the plasma edge. We employ theoretical models for both equilibrium and limiter fields in order to analytically obtain a magnetic field line mapping. In this way the effect of parameter variations is more easily studied in comparison with mappings generated by numerical integration of field line equations.[25] However, the use of very simplified models, with *ad hoc* equilibrium fields and large aspect ratio geometry, may lead to rather artificial mappings which may mask some important aspects of the EML action, such as the role of toroidal effects and the Shafranov shift of magnetic surfaces. We derive a field line mapping which embodies three important features: (i) a coordinate system in which the toroidicity effects appear naturally in the corresponding coordinate surfaces; (ii) a self-consistent equilibrium field obtained from an analytical solution of the Grad–Schlüter–Shafranov equation; (iii) the design of the EML tries to follow the actual helical paths of field lines, taking into account pitch variations due to the toroidal geometry.

The map we obtain is rigorously area preserving, and may be regarded as a canonical transformation between action-angle variables, which are related to the geometrical field-line coordinates.[26] An explicit Hamiltonian function is obtained for the problem, assuming that the EML perturbation is a sequence of delta-function pulses.[27] We analyze phase portraits of this mapping which exhibit a sizable chaotic layer comprising both the plasma edge and the vacuum region that separates it from the inner wall. The radial excursion of chaotic field lines is studied by means of their average square mean displacement. If the chaotic region contains no stable periodic orbits, field line motion is essentially stochastic in the sense that the square mean radial displacement grows linearly with time, the diffusion coefficient being the corresponding growth rate. The presence of periodic islands embedded in the chaotic region alters this situation, however.[28,29] Furthermore, there are other transport regimes—super- and subdiffusive—which are characterized by a power-law dependence on time.[30] Finally, as chaotic field lines diffuse along the radial direction, they eventually collide with the inner wall and are lost. We study statistically this process and find an exponential decay, from which a field line half-life can be defined and studied with respect to variations of the EML current. Moreover, the field line loss process may be treated using Poisson statistics, which is in accordance with the numerical results we obtained.

This paper is organized as follows: In Sec. II we outline the equilibrium and limiter fields to be used in this work. Section III describes the obtention of the field line mapping. Section IV shows results for mean square radial displacement of field lines in predominantly chaotic regions, indicating the transport regimes we observe, as well as the question of the loss of field lines due to collisions with the inner tokamak wall. Section V is devoted to our conclusions.
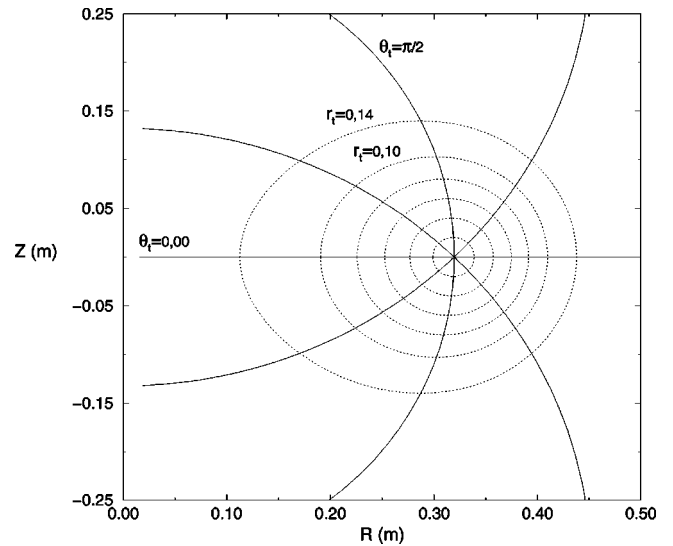

FIG. 1. Some coordinate surfaces of the polar toroidal coordinate system in the $\varphi=0$ plane.

II. EQUILIBRIUM AND LIMITER FIELDS

We use a (nonorthogonal) polar toroidal coordinate system $(r_t, \theta_t, \varphi_t)$ that is introduced to exhibit toroidal effects in the tokamak equilibrium field line geometry.[31] In the large aspect ratio limit these coordinates reduce to the local coordinates (r, θ, φ). For arbitrary aspect ratio they may be defined in terms of the toroidal coordinates (ξ, ω, φ)[32] by the following relations:

$$r_t = \frac{R_0'}{\cosh \xi - \cos \omega}, \tag{1}$$

$$\theta_t = \pi - \omega, \tag{2}$$

$$\varphi_t = \varphi, \tag{3}$$

where R_0' is the magnetic axis radius. In Fig. 1 we depict some of the coordinate surfaces for this system, in the plane $\varphi=0$, and R, Z are usual cylindrical coordinates.

The tokamak equilibrium magnetic field $\mathbf{B}_0$ is obtained from an ideal MHD static equilibrium, described by

$$\mathbf{J} \times \mathbf{B}_0 = \nabla p, \tag{4}$$

$$\nabla \times \mathbf{B}_0 = \mu_0 \mathbf{J}, \tag{5}$$

$$\nabla \cdot \mathbf{B}_0 = 0, \tag{6}$$

where p and $\mathbf{J}$ are the equilibrium pressure and current density, respectively. The equilibrium configuration can be also described by a scalar function Ψ_p, the poloidal magnetic flux function, satisfying

$$\mathbf{B}_0 \cdot \nabla \Psi_p = 0. \tag{7}$$

For an axisymmetric configuration, the poloidal flux is obtained by solving a Grad–Schlüter–Shafranov equation, that is equivalent to Eqs. (4)–(6). In the polar toroidal coordinate system used in this work this equation reads[33]

$$\frac{1}{r_t}\frac{\partial}{\partial r_t}\left(r_t\frac{\partial\Psi_p}{\partial r_t}\right)+\frac{1}{r_t^2}\frac{\partial^2\Psi_p}{\partial\theta_t^2}$$

$$=\mu_0 J_3(\Psi_p)+\mu_0 R_0'^2\frac{dp}{d\Psi_p}\left(2\frac{r_t}{R_0'}\cos\theta_t+\frac{r_t^2}{R_0'^2}\sin^2\theta_t\right)$$

$$+\frac{r_t}{R_0'}\left[\cos\theta_t\left(2\frac{\partial^2\Psi_p}{\partial r_t^2}+\frac{1}{r_t}\frac{\partial\Psi_p}{\partial r_t}\right)\right.$$

$$\left.+\sin\theta_t\left(\frac{1}{r_t^2}\frac{\partial\Psi_p}{\partial\theta_t}-\frac{2}{r_t}\frac{\partial^2\Psi_p}{\partial\theta_t\partial r_t}\right)\right], \tag{8}$$

where J_3 is the toroidal current density, given by

$$J_3(\Psi_p)=-R_0'^2\frac{dp}{d\Psi_p}-\frac{d}{d\Psi_p}\left(\frac{1}{2}\mu_0 I^2\right), \tag{9}$$

in terms of the pressure p and the poloidal current function $I(r_t,\theta_t)$. The contravariant components of the equilibrium magnetic field, consistent with Eq. (7), are

$$B_0^1=-\frac{1}{R_0'r_t}\frac{\partial\Psi_p}{\partial\theta_t}, \tag{10}$$

$$B_0^2=\frac{1}{R_0'r_t}\frac{\partial\Psi_p}{\partial r_t}, \tag{11}$$

$$B_0^3=-\frac{\mu_0 I}{R^2}, \tag{12}$$

where the radial coordinate, in the cylindrical system, is related to the polar toroidal coordinates

$$R^2=R_0'^2\left[1-2\frac{r_t}{R_0'}\cos\theta_t-\left(\frac{r_t}{R_0'}\right)^2\sin^2\theta_t\right]. \tag{13}$$

At the large aspect ratio limit ($r_t\ll R_0'$), and supposing that in lowest order the solution, $\Psi_p(r_t)$, does not depend on θ_t, Eq. (8) reduces to an equilibrium equation similar to the one obtained in a cylindrical geometry, but in terms of r_t.[1] However, as r_t embodies the toroidal character of coordinate surfaces, the intersections of magnetic surfaces $\Psi_p(r_t)$ =const with a toroidal plane are not concentric circles but present a Shafranov shift toward the exterior equatorial region.[31] In this way actual magnetic surfaces are well approximated by coordinate surfaces in which r_t=const.

To solve Eq. (8) we need to assume spatial profiles for both the pressure p and current function I. In lowest order, however, it is sufficient to assume a single profile for the toroidal current density J_3, as given by Eq. (9) in terms of p and I. So, we choose a peaked current profile, commonly observed in tokamak discharges,[1] and given by

$$J_3(r_t)=\frac{I_p R_0'}{\pi a^2}(\gamma+1)\left(1-\frac{r_t^2}{a^2}\right)^\gamma, \tag{14}$$

where I_p and a are the total current and plasma radius, respectively, and γ is a positive constant.

An approximate solution for (8) may be sought in powers of the aspect ratio r_t/R_0'. At lowest order, we find the following equilibrium magnetic field components:[34]

$$B_0^1=0, \tag{15}$$

$$B_0^2=\frac{\mu_0 I_p}{2\pi r_t^2}\left[1-\left(1-\frac{r_t^2}{a^2}\right)^{\gamma+1}\right], \tag{16}$$

$$B_0^3=-\frac{\mu_0 I}{R_0'^2}\left(1-2\frac{r_t}{R_0'}\cos\theta_t\right)^{-1}. \tag{17}$$

The corresponding poloidally averaged safety factor is

$$q=\frac{1}{2\pi}\int_0^{2\pi}\frac{B_0^3(r_t,\theta_t)}{B_0^2(r_t,\theta_t)}d\theta_t=q_c(r_t)\left(1-4\frac{r_t^2}{R_0'^2}\right)^{-1/2}, \tag{18}$$

with

$$q_c(r_t)=-2\pi\frac{I}{I_p}\frac{r_t^2}{R_0'^2}\left[1-\left(1-\frac{r_t^2}{a^2}\right)^{\gamma+1}\right]^{-1}, \tag{19}$$

which results in a parabolic profile. We assume that $q\approx1$ at the magnetic axis and $q\approx5$ at plasma edge. We normalize the minor radius b_t and plasma radius a to the major radius R_0', so that $a/R_0'=0.26$, $b_t/R_0'=0.36$, and $\gamma=3$, which are consistent with typical tokamak discharges.[4] Figure 2(a) shows some equilibrium flux surfaces for this set of parameters, and Fig. 2(b) depicts the corresponding radial profile of the safety factor. In Fig. 2(a), the zeroth- and first-order solutions practically coincide, whereas in Fig. 2(b) they show a small deviation as we approach the plasma edge.

We consider the following design for an ergodic magnetic limiter: N_a current rings of length l located symmetrically along the toroidal circumference of the tokamak (Fig. 3). These current rings may be regarded as slices of a pair of external helical windings located at the tokamak minor radius $r_t=b_t$, and conducting a current I_h in opposite senses for adjacent conductors. To induce a resonant perturbation we choose a helical winding with the same pitch as the field lines in the rational surface we want to perturb. This surface has a safety factor $q=m_0/n_0$, where m_0 and n_0 are positive integers. In order to obtain this effect the winding law takes into account the helical field line pitch nonuniformity caused by the toroidal effect

$$u_t=m_0(\theta_t+\lambda\sin\theta_t)-n_0\varphi_t=\text{constant}. \tag{20}$$

The choice of λ is dictated by the location of the main resonant magnetic surface to be destroyed, and where we aim to produce chaotic field lines. In our case, we chose the resonant effect to occur at the equilibrium rational magnetic surface with $q=5/1$, since it is located near the plasma edge [see Fig. 2(b)]. It corresponds to $\lambda=0.54$, as has been shown in Ref. 34.

The magnetic field produced by the resonant helical winding from which we build the EML rings is obtained by neglecting the plasma response and the penetration time through the tokamak wall. In this case, it is assumed to be a vacuum field: $\mathbf{B}=\nabla\Phi_L$, where the scalar magnetic potential Φ_L satisfies the Laplace equation $\nabla^2\Phi_L=0$ in polar toroidal
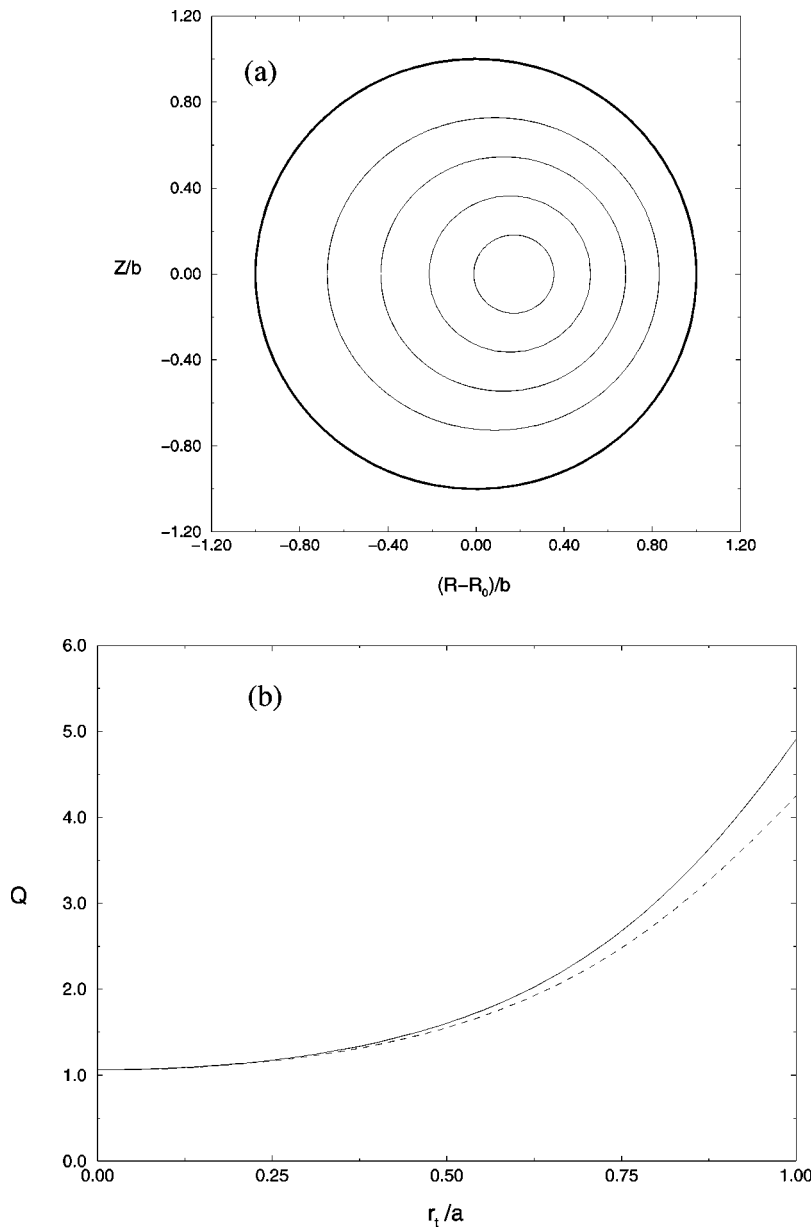
FIG. 2. (a) Equilibrium flux surfaces, and (b) safety factor radial profile for a tokamak. In (b), we show both the zeroth- (dashed line) and first-order (full line) results.

coordinates, and with suitable boundary conditions which take into account the helical conductors at the tokamak wall following the winding law (20). In the following we will rather use the corresponding vector potential $\mathbf{A}_L$, such that $\mathbf{B}_L = \nabla \times \mathbf{A}_L$. In lowest order, the only nonvanishing component of $\mathbf{A}_L$ is

$$A_{L3}(r_t, \theta_t, \varphi_t) = -\frac{\mu_0 I_h R_0'}{\pi} \sum_{k=-m_0}^{+m_0} J_k(m_0 \lambda)$$
$$\times \left(\frac{r_t}{b_t}\right)^{m_0+k} e^{i[(m_0+k)\theta_t - n_0 \varphi_t]}, \quad (21)$$

from which the limiter field components are given by

$$B_L^1 = -\frac{1}{R_0' r_t} \frac{\partial A_{L3}}{\partial \theta_t}, \quad (22)$$

$$B_L^2 = \frac{1}{R_0' r_t} \frac{\partial A_{L3}}{\partial r_t}. \quad (23)$$

Note that, due to the toroidal geometry, a $(m_0, n_0) = (5,1)$ resonant helical winding excites a large number of satellite resonances $(m_0 + k)/n_0$ whose amplitudes, being proportional to Bessel functions of order k, decay with increasing k. Excluding marginal stability states, for which the plasma response would have to be taken into account, the model field is the superposition of the equilibrium and limiter fields: $\mathbf{B} = \mathbf{B}_0 + \mathbf{B}_L$.

III. MAGNETIC FIELD LINE MAPPING

Initially, we consider a tokamak with a resonant helical winding, which is a set of conductor pairs wound around the torus with a given definite pitch that resonates with the rota-
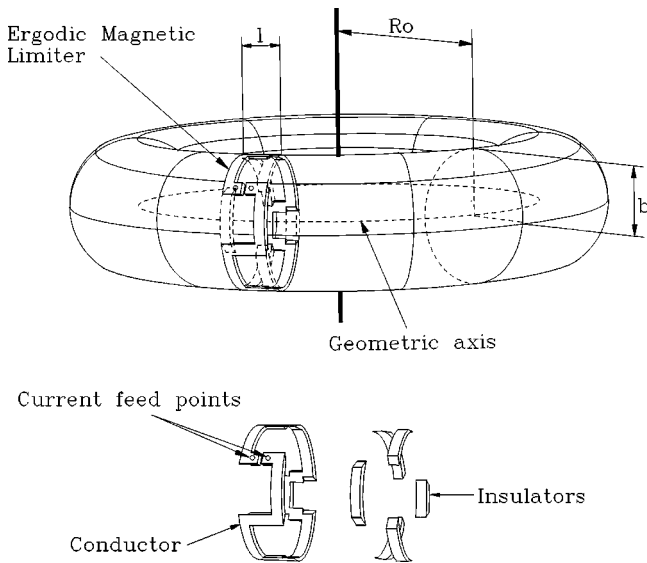
FIG. 3. Schematic diagram of an ergodic magnetic limiter.

tional transform of the magnetic surface we wish to affect. The corresponding magnetic field line equations are written, in toroidal polar coordinates, as

$$\frac{dr_t}{d\varphi_t} = -\frac{1}{r_t B_T}\left(1 - 2\frac{r_t}{R_0'}\cos\theta_t\right)\frac{\partial}{\partial\theta_t}A_{L3}(r_t,\theta_t,\varphi_t), \tag{24}$$

$$\frac{d\theta_t}{d\varphi_t} = \frac{1}{r_t B_T}\left(1 - 2\frac{r_t}{R_0'}\cos\theta_t\right)\frac{\partial}{\partial r_t}[\Psi_p(r_t) + A_{L3}(r_t,\theta_t,\varphi_t)], \tag{25}$$

where we use Eqs. (10)–(12) and (22)–(23), and $B_T \equiv -\mu_0 I/R_0'$ is the toroidal magnetic field at the magnetic axis.

Since the equilibrium field is axisymmetric, we may set the ignorable coordinate φ as a time-like variable, and put field line equations (24) and (25) in a canonical form

$$\frac{d\mathcal{J}}{dt} = -\frac{\partial H}{\partial\vartheta}, \tag{26}$$

$$\frac{d\vartheta}{dt} = \frac{\partial H}{\partial\mathcal{J}}, \tag{27}$$

where $(\mathcal{J},\vartheta)$ are the action-angle variables of a Hamiltonian system and $t\equiv\varphi$. The equilibrium field line Hamiltonian $H = H(\mathcal{J},\vartheta)$ is an autonomous one-degree-of-freedom system, hence it is integrable.[35] The addition of a nonsymmetric perturbation caused by an EML introduces a ''time''-dependent term that breaks the integrability of the system. If the magnitude of this perturbation is not too strong, however, we may use the methods of Hamiltonian dynamics to understand field line behavior.[14]

The action ($\mathcal{J}$) and angle (ϑ) variables are related to the polar toroidal coordinates in the following way:

$$\mathcal{J}(r_t) = \frac{1}{2\pi R_0' B_T}\int\int B_0^3(r_t,\theta_t)r_t\,dr_t\,d\theta_t$$

$$= \frac{1}{4}\left[1 - \left(1 - 4\frac{r_t^2}{R_0'^2}\right)^{1/2}\right], \tag{28}$$

$$\vartheta(r_t,\theta_t) = \frac{1}{q(r_t)}\int_0^{\theta_t}\frac{B_0^3(r_t,\theta_t)}{B_0^2(r_t,\theta_t)}d\theta$$

$$= \left(1 - 4\left(\frac{r_t}{R_0'}\right)^2\right)^{1/2}\int_0^{\theta_t}\frac{d\theta}{1 - 2(r_t/R_0')\cos\theta}$$

$$= 2\arctan\left[\frac{1}{\Omega(r_t)}\left(\frac{\sin\theta_t}{1 + \cos\theta_t}\right)\right], \tag{29}$$

where $t = \varphi$, and

$$\Omega(r_t) = \left(1 - 2\frac{r_t}{R_0'}\right)^{1/2}\left(1 + 2\frac{r_t}{R_0'}\right)^{-1/2}, \tag{30}$$

in such a way that the Hamiltonian for the tokamak field with a resonant helical winding characterized by Eq. (21) is

$$H(\mathcal{J},\vartheta,t) = H_0(\mathcal{J}) + H_1(\mathcal{J},\vartheta,t)$$

$$= \frac{1}{B_T R_0'^2}\Psi_p(\mathcal{J}) + \frac{1}{B_T R_0'^2}A_{L3}(\mathcal{J},\vartheta,t). \tag{31}$$

However, it turns out that the length l of each EML ring is typically a small fraction of the total toroidal circumference $2\pi R_0'$. If l is small enough, we can model its effect as a sequence of delta functions centered at each ring position.[27] So, we suppose the following Hamiltonian for the tokamak with finite length EML rings:

$$H_L(\mathcal{J},\vartheta,t) = H_0(\mathcal{J}) + \frac{l}{R_0'}H_1(\mathcal{J},\vartheta,t)\sum_{k=-\infty}^{+\infty}\delta\left(t - k\frac{2\pi}{N_a}\right), \tag{32}$$

where the N_a rings are symmetrically located along the toroidal direction.

The impulsive character of the perturbation caused by the limiter rings enables us to derive a Poincaré (stroboscopic) map for field line dynamics, defining $\mathcal{J}_n$ and ϑ_n as the action and angle variables at the nth crossing of the plane $\varphi = t = 0$, respectively.[25] In the case of an EML with finite size rings, we have an explicit t dependence in the expressions, that gives a near-integrable Hamiltonian system, if the limiter current is small enough. The canonical area-preserving mapping for this near-integrable system is written as

$$\mathcal{J}_{n+1} = \mathcal{J}_n + \epsilon f(\mathcal{J}_{n+1},\vartheta_n,t_n), \tag{33}$$

$$\vartheta_{n+1} = \vartheta_n + \frac{2\pi}{N_a q(\mathcal{J}_{n+1})} + \epsilon g(\mathcal{J}_{n+1},\vartheta_n,t_n), \tag{34}$$

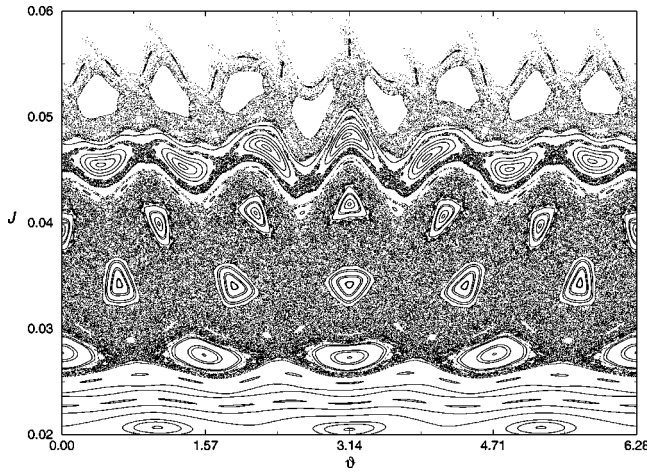$$t_{n+1} = t_n + \frac{2\pi}{N_a}, \tag{35}$$

where

FIG. 4. Phase portrait, in action-angle variables, of the field line map for an EML with $N_a = 4$ rings, $(m_0, n_0) = (5,1)$, $\lambda = 0.54$, and $I_h = 0.021 I_p$.

FIG. 5. Phase portrait, in action-angle variables, of the field line map for an EML with $N_a = 4$ rings, $(m_0, n_0) = (5,1)$, $\lambda = 0.54$, and $I_h = 0.045 I_p$.

$$f(\mathcal{J}, \vartheta, t) = -\frac{\partial H_1(\mathcal{J}, \vartheta, t)}{\partial \vartheta}, \tag{36}$$

$$g(\mathcal{J}, \vartheta, t) = \frac{\partial H_1(\mathcal{J}, \vartheta, t)}{\partial \mathcal{J}}, \tag{37}$$

and the perturbation parameter is

$$\epsilon = -2 \left(\frac{l}{2 \pi R_0'} \right) \left(\frac{I_h}{I} \right). \tag{38}$$

The explicit forms of the Fourier coefficients of H_1 may be found in the Appendix. For $\epsilon = 0$ it results in a radial twist map, characteristic of an integrable system.

In Fig. 4, we show a phase portrait, in action-angle variables, of many orbits with a large number of iterations of the above-mentioned map for an EML with $N_a = 4$ current rings, $(m_0, n_0) = (5,1)$, $\lambda = 0.54$, and a limiter current of 2.1% of the plasma current. There is a main chain of five magnetic islands at $\bar{\mathcal{J}} \approx 0.035$ surrounded by many satellite chains (3/1, 4/1, 6/1, 7/1, and 8/1) caused by toroidicity effects. The overlap of the chains with $m = 4$, 5, and 6 generates a sizable chaotic field line region with a width of $\Delta \mathcal{J} \approx 0.02$ centered at $\bar{\mathcal{J}}$.

This chaotic region does not reach the plasma wall because of some remaining magnetic surfaces that exist between the $m = 6$ and 8 chains, and that act as barriers preventing field line diffusion in the radial direction. In order to have a chaotic region that effectively touches the wall we have to increase the EML current, as shown in Fig. 5, where I_h was raised to 4.5% of I_p. For this higher perturbation value all chains with $m \geq 5$ practically disappear, although the islands' centers—being elliptic (stable) fixed points of the Poincaré map (note the remnant of the $m = 4$ chain)—may still exist, but with a negligible interference on the field line transport.

IV. FIELD LINE DIFFUSION AND LOSS

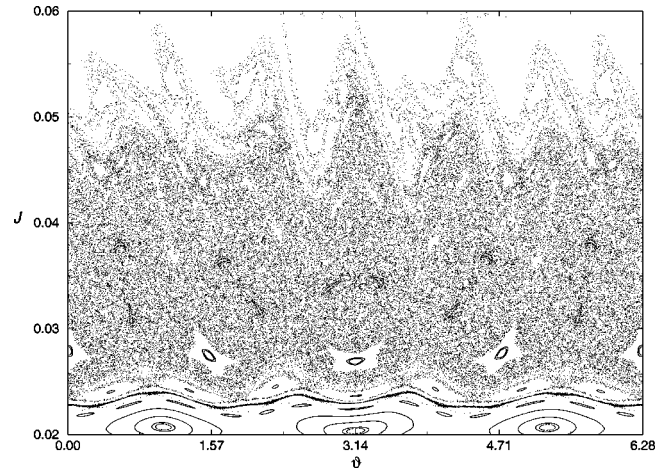The hallmark of chaotic motion in a conservative non-autonomous single-degree-of-freedom system, as is the case

here, is the stretching–folding nature of the dynamics, characterized by the existence of one positive Lyapunov exponent. Since the available phase space is bounded, the result of many stretchings and foldings results in an involved and complex behavior, leading to field line diffusion. However, the phase space structure due to the presence of periodic orbits determines the kind of transport regime we deal with.[28,29] This has been the object of many recent theoretical and numerical studies.[30]

The main function of the EML is to create a boundary layer of chaotic field lines, centered around a given rational magnetic surface that has been destroyed by the perturbation. Throughout this boundary layer, the magnetic field lines show predominantly chaotic, or area-filling, behavior. To study field line diffusion within such a region, we take N_ϑ initial conditions uniformly spread along $\mathcal{J}_{0i} = \bar{\mathcal{J}}$, and $\vartheta_{0i} = 2\pi i / N_\vartheta$, with $i = 1, 2, \ldots N_\vartheta$, and $\bar{\mathcal{J}}$ is picked up from the center of a chaotic region. For each initial condition we compute the average square displacement of the action variable

$$\sigma_n^2 \equiv \langle (\delta \mathcal{J}_n)^2 \rangle_i = \frac{1}{N_\vartheta} \sum_{i=1}^{N_\vartheta} (\mathcal{J}_{ni} - \mathcal{J}_{0i})^2. \tag{39}$$

If the action is not restricted to a limited domain in the Poincaré phase plane $(\mathcal{J}, \vartheta)$ this displacement goes asymptotically as n^μ. Anomalous transport is characterized by $\mu \neq 1$, which we call subdiffusive if $\mu < 1$, and superdiffusive if $\mu > 1$. Gaussian transport is characterized by $\mu = 1$, for which a diffusion coefficient is defined as

$$D_{LF} = \lim_{n \to \infty} \frac{\sigma_n^2}{2n}. \tag{40}$$

As we will see in more detail, it is impossible in practice to take a large time limit in the case of field line transport due to an EML, since field lines eventually collide with the tokamak wall and are lost. To circumvent this problem it is possible to consider the diffusion only in a limited region in action space. The diffusion coefficient, in this case, is pro-
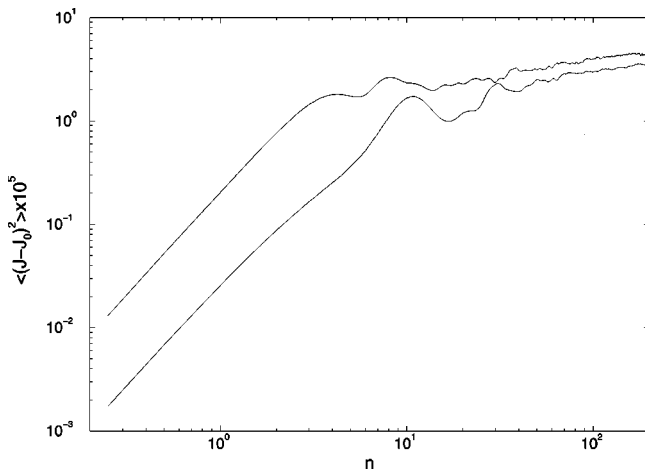
Phys. Plasmas, Vol. 8, No. 6, June 2001

Field line diffusion and loss in a tokamak   2861

FIG. 6. Time evolution of the average square action displacement for an EML with $(m_0,n_0)=(5,1)$, $\lambda=0.54$, and two different limiter currents: $0.045I_p$ (upper curve) and $0.021I_p$ (lower curve). n is the number of toroidal turns.

portional to the ratio between the action interval $\Delta\mathcal{J}$ and the average number of field line turns in the toroidal direction.

The anomalous, or non-Gaussian, nature of field line transport due to EML may be seen in Fig. 6, where the time behavior of the average square displacement σ_n^2 is depicted for two different values of the EML current, corresponding to the phase portraits of Figs. 4 and 5. We used $N_\vartheta=4000$ initial conditions at $\bar{\mathcal{J}}=0.031$ and spread out uniformly along the ϑ direction. We see that for both EML current values the transport is initially superdiffusive, with σ_n^2 growing with time roughly as $n^{1.8}$. After only a dozen iterations, however, the field line transport becomes subdiffusive. The fact that the process is not Gaussian indicates that the chaotic region contains islands which have a trapping effect on field lines. A chaotic field line that approaches the remnant of an island would stay around it for a given time before entering in the neighborhood of another island, and so on.

In order to visualize the trapping effect caused by the islands embedded in the chaotic region on the field line dynamics, we show in Fig. 7 the forward images, after 5 and 15 iterations, respectively, of a bunch of initial conditions at $\bar{\mathcal{J}}=0.031$ and uniformly distributed along the poloidal direction, with an EML current of $I_h=0.021I_p$. We may observe the stretching and folding nature of the bounded dynamics with positive Lyapunov exponent in the chaotic region. The foldings are modulated by the presence of the island remnants. This highly convoluted set, formed by the forward images of the initial conditions chosen, may reach the inner wall at $r_t=b_t$ after a large number of iterations, which will cause loss of field lines.

This also causes σ_n^2 to decrease for large times, provided the chaotic region reaches $r_t=b_t$, complicating an analysis of the diffusive behavior. This is shown in Fig. 8, where we plot in grayscale the time (in number of toroidal turns) it takes for a field line to reach the tokamak wall. The EML current here is increased to 5.0% of I_p. The darker the phase space point, the larger the time required for a field line starting at that point to hit the wall. The presence of islands
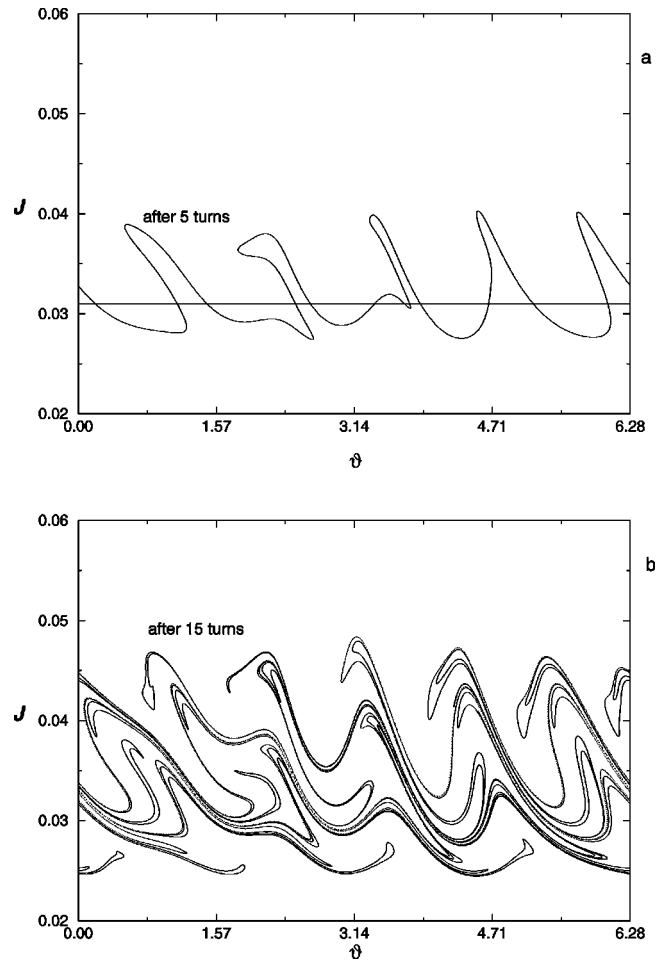

FIG. 7. Forward images, after 5 and 15 iterations, of a bunch of initial conditions within the chaotic region, for the same parameters as in Fig. 4.

embedded in this chaotic sea is clearly inferred from the highly convoluted regions characterized by high escape times, since these islands delay field line escape and eventual loss. The presence of white tongues indicates that the escape pattern is more akin to a convective transport than to a diffusive one, since in the latter case we would expect a more uniform escape pattern due to the ergodic nature of the Gaussian transport process.

A field line is considered lost whenever it reaches the tokamak wall at $\mathcal{J}\approx0.06$. This causes the decrease of the mean square displacement σ_n^2 for large times. In Fig. 9, we plot the fraction of lost field lines N_{LF} (with respect to the total number of initial conditions N_T used to iterate the field line map) as a function of the number of toroidal turns, for $I_h=0.045I_p$. We emphasize that, as we have four limiters, the time is discretized corresponding to an excursion of a quarter of turn (i.e., there are four points for each complete toroidal turn). This decay process is well fitted by an exponential law

$$N_{LF}(n)=N_T\exp\left(-\frac{n-n_0}{\bar{n}}\right),\qquad(41)$$

in which $N_T=4000$, $n_0=69$, and $\bar{n}=2393$. The process resembles the exponential decay of a radioactive nuclei, and accordingly we may compute its half-life $T_{1/2}$, or the time it
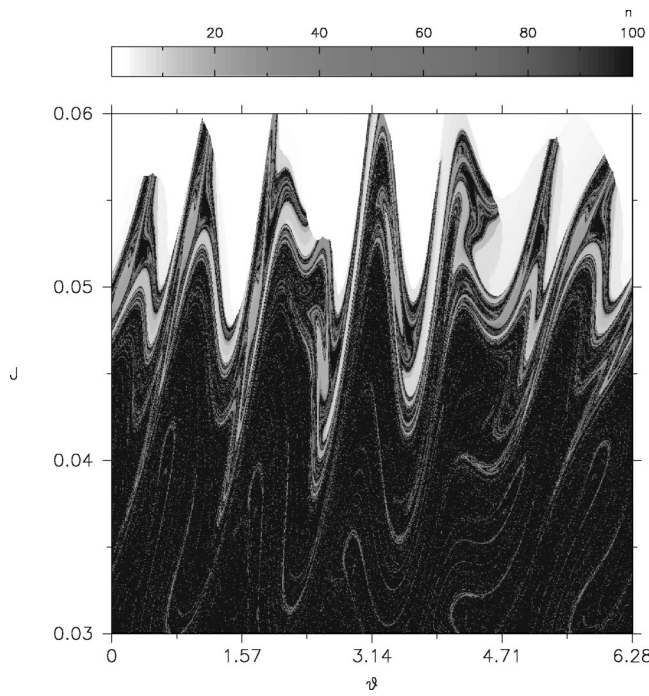
FIG. 8. Grayscale plot of escape times for chaotic field lines generated by an EML with $(m_0, n_0) = (5,1)$, $\lambda = 0.54$, and $I_h = 0.050 I_p$.

takes to decrease the number of remaining field lines to half of their initial values. From Fig. 9, we see that $T_{1/2} \approx 1700$ for the limiter current used there. In Fig. 10, this half-life is plotted *versus* the relative limiter current. The solid line is a power-law scaling $T_{1/2} = a_1 I_h^{-r_1}$, where $a_1 = 3.10 \times 10^8$, and $r_1 = 8.42$. Since the increase of the EML current enhances the diffusion process itself, field lines are more rapidly lost, thus lowering the corresponding half-life.

As with a radioactive decay, the statistical process of field line loss is described by two events: a field line hits or does not hit the tokamak wall, and the probability $p_\alpha(m)$ of hitting the wall is much lower than the probability $1 - p_\alpha(m)$ of not doing so. This suggests a Poisson probability distribution[36]

FIG. 10. Half-life of field lines as a function of limiter current for an EML with $(m_0, n_0) = (5,1)$, and $\lambda = 0.54$.

$$P_\alpha(m) = \frac{1}{m!} e^{-\alpha T} (\alpha T)^m, \tag{42}$$

that, during the observation time T (measured in number of toroidal turns), m field lines are lost. For this reason, α may be called a field line decay rate.

We choose each interval T to correspond to two toroidal turns, for $N_0 = 500$ observations (or 1000 turns). From the obtained values of m, we make a frequency histogram (Fig. 11), where the white bars represent the statistics obtained through N_0 observations of lost field lines. Denoting $\langle m \rangle$ the average value of the number of lost field lines we have, for this Poisson distribution, that $\langle m \rangle = \alpha T \approx 1.90$. Black bars show the corresponding results for Eq. (42). We have a good agreement between a Poisson distribution and the numerically determined frequency histogram, since the statistical uncertainty in the latter may be estimated as $[N_0 p_\alpha(m)(1 - p_\alpha(m))]^{1/2}$, and the differences between our numerical results and those given by Eq. (42) differ by less than one standard deviation. We have also computed higher moments
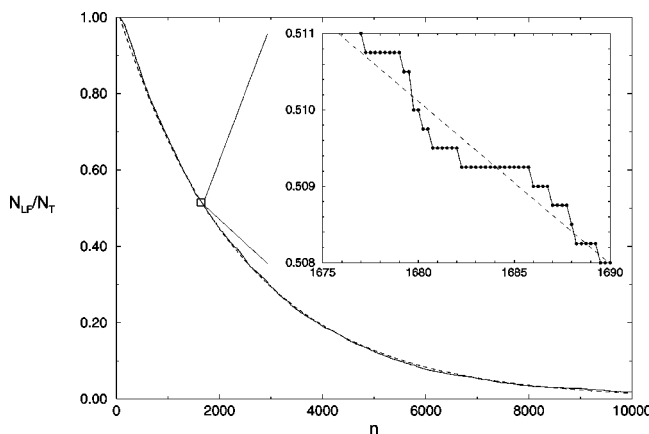

FIG. 9. Fraction of lost field lines due to an EML with $N_a = 4$ rings, $(m_0, n_0) = (5,1)$, $\lambda = 0.54$, and $I_h/I_p = 0.045$. The dashed line corresponds to Eq. (41). The inset shows that the decay process has a staircase behavior.
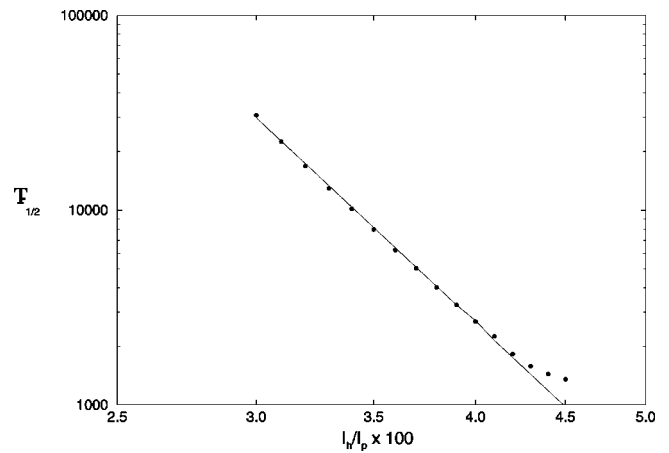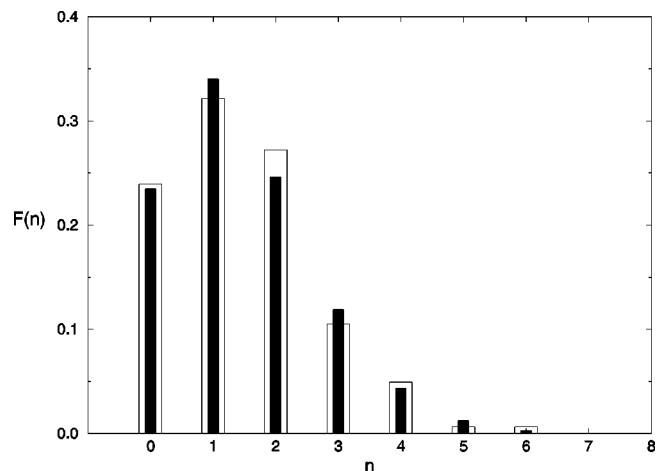

FIG. 11. Number of observations (each observation corresponds to two toroidal turns) in which n field lines were lost, for a (5,1) limiter, with $\lambda = 0.54$ and $I_h/I_p = 0.045$. White and black bars correspond to numerical results and a Poisson distribution, respectively.

Phys. Plasmas, Vol. 8, No. 6, June 2001

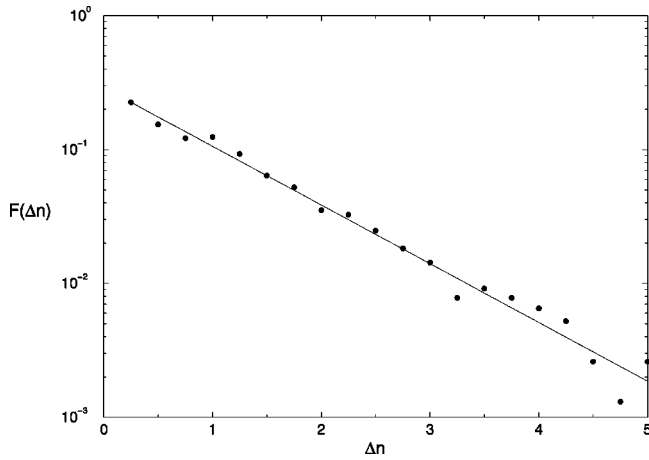Field line diffusion and loss in a tokamak   2863

FIG. 12. Frequency histogram for the plateau lengths in the field line decay produced by a (5,1) limiter, with $\lambda = 0.54$ and $I_h/I_p = 0.045$. The solid line corresponds to Eq. (45).

of the distribution, the asymmetry $S(m)$ and kurtosis $K(m)$, to be 0.84 and 3.72, respectively. These values are close to the corresponding values predicted for a Poisson distribution, namely

$$S(m) = \frac{1}{\sqrt{\langle m \rangle}} = 0.73, \tag{43}$$

$$K(m) = 3 + \frac{1}{\langle m \rangle} = 3.53. \tag{44}$$

The exponential decay of chaotic field lines due to collisions with the tokamak wall may be considered in more detail. From the inset in Fig. 9 we see that this decay is not continuous, but rather is a process in which there are many plateaus with different lengths. In Fig. 12, we show a distribution of the time intervals between successive losses of field lines, which is a normalized frequency histogram of the plateau lengths. $F(\Delta n)$ denotes the relative number of plateaus with length Δn. For a given EML current we have far more small plateaus (in which field line loss occurs after a few toroidal excursions) than long plateaus.

This probability distribution is well fitted by an exponential function

$$F(\Delta n) = \kappa e^{-\kappa \Delta n}, \tag{45}$$

from which we can compute averages, as for the plateau length

$$\langle \Delta n \rangle = \int_0^\infty d(\Delta n) F(\Delta n) \Delta n = \frac{1}{\kappa}, \tag{46}$$

assuming proper normalization for $F(\Delta n)$. From the data shown in Fig. 12, we obtain an average plateau length of $\langle \Delta n \rangle \approx 1.11$, so that $\kappa \approx 0.90$. On the other hand, comparing this exponential fit with the Poisson distribution (42) we have that $\kappa = \alpha = 0.95$. The agreement between these two estimated values of κ is a further evidence that the field line loss is a process described by a Poisson statistics.

One remark should be made here. If we observe for a long time the number of field lines that remain in the chaotic region, the decay rate α will change as the numerical experiment goes on. As a consequence, the number of field lines that hit the wall, over an observation interval T, does not strictly obey a Poisson distribution law. However, if we divide the total observation period into N shorter intervals, in each of them the Poisson statistics may still hold. The corresponding decay rates α_i, $i = 1, 2, \ldots N$, will generally be different, but being Poissonian the overall collision rate will be the sum of the individual rates: $\alpha = \alpha_1 + \alpha_2 + \cdots \alpha_N$.

V. CONCLUSIONS

The ergodic magnetic limiter (EML) is designed to provide a cold boundary layer of chaotic magnetic field lines in the periphery of the tokamak plasma column. In practice this means a region of predominantly chaotic field lines which comprises both the plasma edge and the vacuum scrape-off layer that embraces it. The presence of this chaotic region is achieved by creating adjacent chains of magnetic islands, each of them with their own local chaotic region surrounding the separatrices. These local regions may coalesce and form a large-scale chaotic region through which field lines diffuse. If the chaotic region is large enough, they may collide with the tokamak inner wall and are eventually lost.

The study of field line transport in such chaotic regions and their loss due to collisions with the wall depends on long-term integration of magnetic field line equation. An analytically obtained mapping is a convenient tool to analyze field line behavior for a large number of turns. Using a convenient coordinate system (polar toroidal), we derive a map whose coordinate surfaces are good candidates for equilibrium flux surfaces, in the sense that they present a Shafranov shift. Another feature of our model is the use of an equilibrium field that results from an approximate analytical solution of the Grad–Schlüter–Shafranov equation, and by adopting a current density model that yields a parabolic safety factor profile.

The EML design that we consider embodies a parameter λ introduced to make the distribution of external conductors match the actual field line paths. The magnetic field of such a configuration is obtained by using the same geometry as for the equilibrium field. The use of a nonzero λ enhances the resonant effect of the EML. For example, a (5/1) EML with $\lambda \neq 0$ and a MHD equilibrium with $q \approx 5.0$ at the plasma edge give a sizable chaotic region centered at the plasma edge, and reaching the inner wall.

Our results show that there are two transport regimes for the chaotic region at the edge. Initially, a superdiffusive regime appears as a result of a positive Lyapunov exponent, leading to stretching and subsequent folding of bunches of field lines. After a few iterations, the existence of island chains causes a trapping effect, limiting field line excursions, and leading to a subdiffusive regime. A similar investigation for the diffusivity of field lines in a tokamak with ergodic divertor, in a cylindrical geometry, has shown a subdiffusive regime only.[37] In this paper we consider another kind of resonant perturbation, and the mapping is obtained for a toroidal geometry.

The field line loss is described by an exponential-type decay. This decay, however, if viewed in detail is not continuous, but rather occurs in plateaus, whose lengths were found to obey a Poisson statistics. Moreover, the half-life of a diffusing field line depends on the limiter current in a power-law fashion.

APPENDIX: EXPLICIT FORM OF THE FIELD LINE MAP FUNCTIONS

In this appendix we outline the explicit form of the functions f and g that appear in the field line map. The Hamiltonian characterizing the EML field may be Fourier-expanded in the action-angle variables of the unperturbed problem as

$$H_1(\mathcal{J},\vartheta,t) = \sum_{m'=0}^{2m_0} H_{m'}(r_t(\mathcal{J})) e^{i[m'\theta_t(\mathcal{J},\vartheta) - n_0 t]}, \quad (A1)$$

with coefficients given by

$$H_{m'}(r_t) = -J_{m'-m_0}(m_0\lambda)\left(\frac{r_t}{b_t}\right)^{m'}. \quad (A2)$$

It is convenient to rewrite (A1) in the form

$$H_1(\mathcal{J},\vartheta,t) = \sum_{n=0}^{2m_0} H_n^*(\mathcal{J}) e^{i(n\vartheta - n_0 t)}, \quad (A3)$$

where the coefficients are

$$H_m^*(\mathcal{J}) = \sum_{m'=0}^{2m_0} H_{m'}(r_t(\mathcal{J})) S_{m,m'}(\mathcal{J}), \quad (A4)$$

where

$$S_{m,m'}(\mathcal{J}) = (-1)^m \left(\frac{c_1(\mathcal{J})}{c_2(\mathcal{J})}\right)^{m+m'} \sum_{n=0}^{m} (-1)^n \alpha_n(m,m')$$
$$\times \left(\frac{c_1(\mathcal{J})}{c_2(\mathcal{J})}\right)^{-2n}, \quad (A5)$$

with

$$c_1(\mathcal{J}) = 1 - \frac{1}{\Omega(r_t(\mathcal{J}))}, \quad (A6)$$

$$c_2(\mathcal{J}) = 1 + \frac{1}{\Omega(r_t(\mathcal{J}))}, \quad (A7)$$

$$\alpha_n(m,m')$$
$$= \begin{cases} 1 & \text{if } m=0 \quad \text{and } n=0 \\ m' & \text{if } m=1 \quad \text{and } n=0 \quad \text{or } n=11 \\ m'\dfrac{(m+m'-n-1)!}{(m-n)!(m'-n)!n!} & \text{if } m>1 \quad \text{and } n\leq m' \\ 0 & \text{if } m>1 \quad \text{and } n>m'. \end{cases}$$
$$(A8)$$

[1] J. P. Freidberg, *Ideal Magnetohydrodynamics* (Plenum, New York, 1987).
[2] J. Wesson, *Tokamaks* (Oxford University Press, Oxford, 1987).
[3] P. J. Morrison, Rev. Mod. Phys. **70**, 467 (1998).
[4] A. J. Wooton, B. A. Carreras, H. Matsumoto, K. McGuire, W. A. Peebles, Ch. P. Ritz, P. W. Terry, and S. J. Sweben, Phys. Fluids B **2**, 2879 (1990).
[5] F. Wagner and U. Stroh, Plasma Phys. Controlled Fusion **35**, 1321 (1993).
[6] J. D. Meiss, Rev. Mod. Phys. **64**, 795 (1992).
[7] D. F. Düchs, A. Montvai, and C. Sack, Plasma Phys. Controlled Fusion **33**, 919 (1991).
[8] M. N. Rosenbluth, R. Z. Sagdeev, J. B. Taylor, and G. M. Zaslavsky, Nucl. Fusion **6**, 297 (1966).
[9] J. M. Finn, Nucl. Fusion **15**, 845 (1975).
[10] A. S. Fernandes, M. V. A. P. Heller, and I. L. Caldas, Plasma Phys. Controlled Fusion **30**, 1203 (1988).
[11] L. H. A. Monteiro, V. Okano, M. Y. Kucinski, and I. L. Caldas, Phys. Lett. A **193**, 89 (1994).
[12] D. Biskamp, *Nonlinear Magnetohydrodynamics* (Cambridge University Press, Cambridge, 1993).
[13] B. V. Chirikov, Phys. Rep. **52**, 265 (1979).
[14] A. J. Lichtenberg and M. A. Lieberman, *Regular and Chaotic Dynamics,* 2nd ed. (Springer, New York, 1992).
[15] K. M. McGuire and D. C. Robinson, in *Proceedings of the Ninth European Conference on Controlled Fusion and Plasma Physics, 1979* (European Physical Society, Petit-Lancy, 1979), Vol. 1.
[16] D. C. Robinson, Nucl. Fusion **25**, 1101 (1985).
[17] F. Karger and K. Lackner, Phys. Lett. A **61**, 385 (1977); W. Engelhardt and W. Feneberg, J. Nucl. Mater. **76–77**, 518 (1978).
[18] W. Feneberg, in *Proceedings of the Eight European Conference on Controlled Fusion and Plasma Physics, 1977* (European Physical Society, Petit-Lancy, 1977), Vol. 1, p. 3.
[19] W. Feneberg and G. H. Wolf, Nucl. Fusion **27**, 669 (1981).
[20] T. J. Martin and J. B. Taylor, Plasma Phys. Controlled Fusion **26**, 321 (1984).
[21] N. Ohyabu, J. S. deGrassie, N. H. Brooks *et al.*, J. Nucl. Mater. **121**, 363 (1984).
[22] M. S. T. Araújo, A. Vannucci, and I. L. Caldas, Nuovo Cimento D **18**, 807 (1996).
[23] S. Takamura, Y. Shen, H. Yamada *et al.*, J. Nucl. Mater. **162–164**, 643 (1989).
[24] Y. Shen, M. Miyake, S. Takamura *et al.*, J. Nucl. Mater. **168**, 295 (1989).
[25] I. L. Caldas, J. M. Pereira, K. Ullmann, and R. L. Viana, Chaos, Solitons Fractals **7**, 991 (1996).
[26] K. Ullmann and I. L. Caldas, Chaos, Solitons Fractals **11**, 2129 (2000).
[27] R. L. Viana and D. B. Vasconcelos, Dynam. Stabil. Syst. **12**, 75 (1997).
[28] J. D. Meiss, J. R. Cary, J. D. Crawford, C. Grebogi, A. N. Kaufman, and H. D. I. Abarbanel, Physica D **6**, 375 (1983).
[29] R. D. Hazeltine and J. D. Meiss, *Plasma Confinement* (Addison–Wesley, Reading, MA, 1992).
[30] I. Doxas, W. Horton, and H. L. Berk, Phys. Fluids A **2**, 1906 (1990); D. K. Chaiklovsky and G. M. Zaslavsky, Chaos **1**, 463 (1991); R. Balescu, Phys. Rev. E **58**, 3781 (1998).
[31] M. Y. Kucinski and I. L. Caldas, Z. Naturforsch., A: Phys. Sci. **42**, 1124 (1987).

Phys. Plasmas, Vol. 8, No. 6, June 2001

Field line diffusion and loss in a tokamak 2865

[32] P. M. Morse and H. Feshbach, *Methods of Theoretical Physics* (McGraw–Hill, New York, 1953), Vol. 2.

[33] M. Y. Kucinski, I. L. Caldas, L. H. A. Monteiro, and V. Okano, J. Plasma Phys. **14**, 303 (1990).

[34] E. C. da Silva, I. L. Caldas, and R. L. Viana, ''The structure of chaotic magnetic field lines in a tokamak with external nonsymmetric magnetic perturbations,'' IEEE Trans. Plasma Sci. (to be published).

[35] K. J. Whiteman, Rep. Prog. Phys. **40**, 1033 (1977).

[36] M. G. Bulmer, *Principles of Statistics* (Dover, New York, 1979).

[37] S. S. Abdullaev, K. H. Finken, A. Kaleck, and K. H. Spatschek, Phys. Plasmas **5**, 196 (1998).